A Multi-State Empirical Valence Bond Model for Weak Acid Dissociation in Aqueous Solution†

Martin Čuma, Udo W. Schmitt, and Gregory A. Voth*

Department of Chemistry and Henry Eyring Center for Theoretical Chemistry, 315 S. 1400 E. Rm 2020, University of Utah, Salt Lake City, Utah 84112-0850

Received: October 17, 2000

The development and application of a multistate empirical valence bond (MS-EVB) model for a weak acid dissociation and subsequent proton transport in aqueous solution is described. The weak acid dissociation step is modeled by the inclusion of an additional EVB state describing the case when proton is bound to the acid's conjugate base. The model was parametrized for the imidazolium cation deprotonation. Classical molecular dynamics simulation methodology was used to study both equilibrium and dynamic properties of this system. Free energy profiles of the deprotonation reaction, studied using a novel center of excess charge reaction coordinate, reveal the need to include several solvation shells around the weak acid in order to stabilize the hydronium species formed upon the weak acid deprotonation. The solvent atomic density plots examined at selected points along the proton transfer coordinate display a relatively large reorganization of the solvent around the weak acid molecule, caused by the shift in the weak acid molecule atomic point charges caused by the deprotonation. Finally, since the concentration of the weak acid in the system under study is low, its presence has only mimimal effect on the solvent diffusion and on the transfer dynamics of the excess proton in the water solution after the weak acid dissociation step.

1. Introduction

Due to their intrinsic importance, acid−base reactions in aqueous solution and the associated proton transfer and transport (PT) processes have been a subject of intensive research over decades.[1−4] With the improvements in simulation methods[5−7] and the enormous increase in computing power, computational modeling has proven to be a valuable tool in the understanding the microscopic nature of PT reactions.

Empirical potential energy functions have been used extensively in connection with classical molecular dynamics (MD) to study solvated ions in water;[8,9] however, modeling of the ionization process itself is inherently difficult due to the need to allow for the breaking and formation of chemical bonds during the reaction process. The process of bond dissociation can be successfully studied by utilizing molecular dynamics based on electronic structure methods, e.g., the Car−Parrinello approach.[10,11] However, these methods require an explicit treatment of the electronic degrees of freedom and therefore are very costly for systems consisting of more than several tens of water molecules. There is also the issue of the accuracy of the underlying electronic density functional used in such approaches.

Therefore, there is a continuing trend to improve the PT reaction potentials based on molecular mechanics force fields to allow for chemical bond rearrangements. One way to effectively include the bond breaking and formation into potential energy models is provided via the empirical valence bond (EVB) method, introduced by Coulson[12] and Mulliken[13] and further developed and extensively applied by Warshel.[6,14,15] This method is based on the assumption that the ground state of a reactive system can be described as a linear combination of several empirical valence bond (VB) states that correspond to the reactants and products involved in the reaction. For example, in the case of acid dissociation

$$HA + H_2O \rightarrow A^- + H_3O^+ \qquad (1)$$

one VB state would describe the reactant system $HA + H_2O$ and a second VB state the products $A^- + H_3O^+$. The matrix elements entering the associated VB eigenvalue problem are usually modeled by established classical MD force fields, and the coupling between them is chosen so that the ab initio ground state potential energy surface (PES) of the process is reasonable well reproduced in critical regions of the configurational space. Due to its simplicity, the EVB method is numerically inexpensive, and provided that appropriate functional forms and parameters describing the matrix elements can be found, the modeling results can be at a quantitative level.

Recently, a multistate empirical valence bond (MS-EVB) model for proton transport in water was developed in our group,[16−18] which successfully reproduces various important aspects of this elementary process. As was also shown recently,[19] it turns out to be relatively straightforward to insert a counterion into a protonated water solution within this MS-EVB model. A similar model, which differs in important ways,[16−18] has been developed by Borgis and co-workers.[20−23]

With regard to acid−base reactions, however, our original MS-EVB approach allows one to only study the proton migration after the initial PT step from the acid species into the aqueous solution. This can be a realistic approximation for strong acids, which have large dissociation constants and therefore a short lifetime of the ion contact pair. In the case of weak acids, on the other hand, the ionization step needs to be included explicitly into the EVB model because their dissociation constant is small and there is a nonnegligible lifetime of either the solvated acid [HA in eq 1] or the contact ion pair

† Part of the special issue "William H. Miller Festschrift".

10.1021/jp0038207 CCC: $20.00
Published on Web 02/24/2001

$H_3O^+A^-$ in the solution. The explicit treatment of acid dissociation can be readily achieved by the inclusion of an additional VB state that describes the hydrated acid molecule within the MS-EVB description for proton transport through water. We have recently presented an initial study outlining this approach,[19] and the aim of this paper is to provide an extended examination of our augmented MS-EVB model which is capable of modeling weak acid dissociation.

As a model system for weak acid dissociation, the deprotonation of the imidazolium cation (ImH^+) in aqueous solution has been chosen, which yields a neutral imidazole molecule (Im) and a hydronium ion, i.e.

$$ImH^+ + H_2O \rightarrow Im + H_3O^+ \tag{2}$$

Imidazole is a heteroaromatic molecule with one basic nitrogen and one acidic NH group, which constitutes a building block for several biologically important organic molecules, e.g., the amino acids tryptophan and histidine. Histidine is found in the active sites of various enzymes and is believed to play a crucial role in their catalytic behavior.[6] Since most of the enzymatic catalytic processes proceed at a room temperature in an aqueous environment, a good theoretical description of the imidazole interactions with water molecules involved in its protonation and deprotonation will necessary to accurately study enzymes.

Protonation of imidazole has been previously studied using ab initio methods in gas phase and solution[24−26] and also via QM/MM free energy perturbation molecular dynamics.[27,28] The treatment of long-range electrostatic interactions in an MD simulation of Im and ImH^+ in liquid bulk phase water was also discussed recently.[29] These past studies form a good basis for a general understanding of the PT process in extended water−imidazole systems, but they did not focus in detail on the actual deprotonation step of imidazolium in aqueous solution. The main goal of this study is thus to develop a PES model based on the MS-EVB methodology that correctly describes the PT process from ImH^+ into its hydration shells in both gas phase and bulk aqueous solution.

Our interest in the imidazolium deprotonation stems from an ongoing effort to study the catalytic mechanism of the enzyme carbonic anhydrase (CA).[30−32] In several variants of this enzyme, the rate-limiting step in the catalysis is considered to be a proton transfer from the active site to a histidine ligand,[30] which proceeds via a hydrogen bonded water bridge consisting of several water molecules. The last step of this reaction, protonation of the histidine residue, can be approximated by the protonation of the imidazole molecule, as imidazole forms the active site of the histidine residue. An accurate description of the PT mechanism in both bulk phase water and for the hydrated imidazole will be essential to reasonably model the water bridge proton shuttle process in the enzyme. The first requirement is already provided per se by our previous proton-transfer MS-EVB model.[16−18] The development and parametrization of an augmented EVB model for the imidazole protonation-deprotonation process thus remains the focus of this study. The imidazolium molecule consists of two acidic NH groups, which are equivalent. However, in the protein environment, one of the groups is usually screened by neighboring residues and therefore does not participate in the PT process. This is also the case in CA. Consequently, only one proton donor NH group will be included in the EVB description of the imidazolium cation.

The paper is structured as follows. The next section includes a brief summary of the MS-EVB method with details on the weak acid MS-EVB model parameter set. Section 3 presents results of the ab initio PES calculations of small ImH^+−water clusters and a description of the parametrization procedure of the weak acid EVB potential. Section 4 describes the MD simulation strategies using the weak acid MS-EVB model, while results are presented and discussed in Section 5. Conclusions are given in Section 6.

2. Theoretical Model

A. Summary of the Model. The theoretical background of the MS-EVB model has been discussed in detail in previous publications.[16−18] In short, the ground state PES of the reacting system can be obtained from appropriately chosen localized valence bond states as the lowest eigenvalue $E_0(\mathbf{x})$ of the $N \times N$ EVB Hamiltonian

$$\mathbf{H} = \sum_{i,j} |i\rangle\, h_{ij}(\mathbf{x})\, \langle j| \tag{3}$$

where h_{ii} corresponds to the potential energy of the VB state $|i\rangle$ and h_{ij} is the coupling between the VB states $|i\rangle$ and $\langle j|$. The vector $\mathbf{x}$ represents the complete set of nuclear degrees of freedom. The diagonal matrix elements are described by molecular mechanics force fields while the off-diagonal elements are determined empirically to correctly mimic the PES of the system under consideration. Note that the coupling term is present only between the VB states that are allowed to chemically react with each other. For example, in the weak acid EVB model, the weak acid VB state $|a\rangle$ is coupled only to one hydronium VB state $|b\rangle$ formed by the acid's proton and the water molecule that hydrates it.

An important feature in the MS-EVB model for proton transport in water developed in our group[16−18] is that it treats the solvent−solute charge interactions in both the diagonal and off-diagonal element of the hydronium EVB states. The off-diagonal or exchange charge distribution is included to describe the nonvanishing off-diagonal overlap of the individual VB electronic states in the protonated water solution. Due to the more complex charge distribution on the imidazole molecule, no attempt was made at this time to include this term into the weak acid−water coupling element. Thus, the solute−solvent electrostatic interactions in this VB state consist only of the atomic point charges in the diagonal potential terms. However, the exchange interaction remains included in the coupling of the states describing the structure and transport of the hydrated proton.

B. Hydronium VB State. In the following, the implementation details of the MS-EVB model for weak acids will be given with special emphasis on the differences from the original MS-EVB model.[16−18] The EVB states representing the protonated water with a conjugate base of a weak acid (A^-, or Im in this work), also denoted below as the hydronium VB state, required several modifications in the calculation of the diagonal EVB matrix elements. One of these states is schematically depicted in the upper panel of Figure 1. As a start, the imidazole molecule force field and its interaction with the solvent must be added to the diagonal matrix term. The intramolecular potential of an Im molecule is described by harmonic bond and bend terms, whereas the torsion terms are based on truncated Fourier series. Furthemore, nonbonded interactions between the nonadjacent atoms (1−4 terms) are included. The nonbonded intramolecular and the water/hydronium-imidazole nonbonding intermolecular interactions are modeled by standard Lennard−Jones (LJ) and Coulombic potential terms. The intramolecular and LJ force field form and parameters for the imidazole molecule are the same

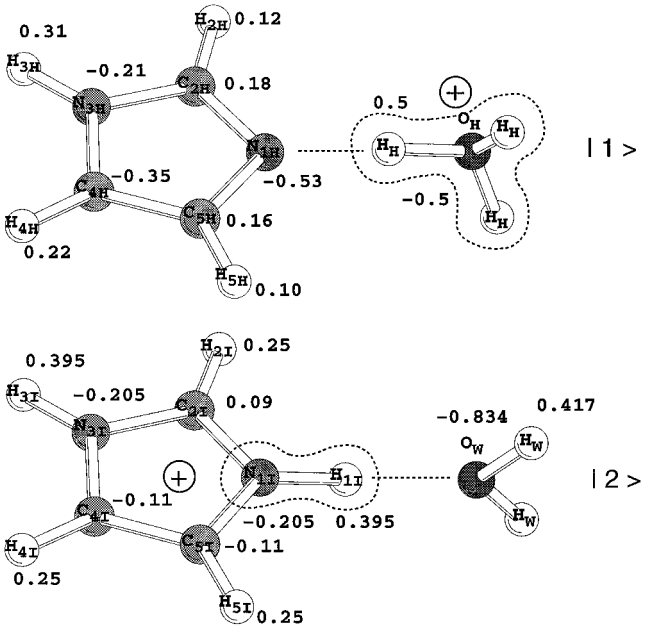

Figure 1. Schematic picture of the imidazole, $Im-H_3O^+$ $|1\rangle$ and imidazolium, $Im-H_3O^+$ $|2\rangle$ VB states with charges used in the MS-EVB model.

as those in our previous publication[19] and were taken from the CHARMM histidine residue parameter set.[33] The imidazole atomic charges, however, were modified. In this work, we use more realistic point charges calculated from the electrostatic charge distribution according to the Merz−Kollman scheme,[34] evaluated at the ab initio HF/6-31G* level. Charges for the hydronium VB state are included in Figure 1 for VB state $|1\rangle$. As in the previous work, a hydronium H atom LJ term is included in the interaction with the imidazole to compensate for the affinity between the imidazole N proton acceptor atom and the hydronium hydrogens. The hydrogen LJ parameters were taken to be $\sigma = 0.40$ Å and $\epsilon = 0.046$ kcal mol^{-1}.

As mentioned in our earlier publication,[19] in the case of the hydronium VB state, the major difference between the original protonated water MS-EVB model[16−18] and the one used in this work is that the water molecules interacting with the hydronium use the full charges as opposed to the charge-scaling procedure introduced in ref 17. We will hereafter refer to the new MS-EVB model for the hydrated proton as the "MS-EVB2" model. Several terms in the MS-EVB2 parameter set were modified to reproduce the energetics and geometry of the small protonated water clusters. In a future publication, we will describe the MS-EVB2 model in detail as well as point out the small differences in static and dynamic characteristics between the two models. The present MS-EVB2 hydronium VB state parameter set is also slightly modified from the one presented before.[19] For consistency, we list here all the changes introduced on the hydronium VB terms from the original charge-scaled MS-EVB parametrization.[17]

The intermolecular interactions of the hydronium species with surrounding water molecules are described in the MS-EVB2 model by

$$V^{\text{inter,k}}_{H_3O^+,H_2O} = V_{\text{Coulomb}} + V_{\text{LJ}} + V^{\text{rep}}(R_{OO_k}) + V^{\text{rep}}(R_{OH_k}) \quad (4)$$

The terms V_{Coulomb} and V_{LJ} represent Coulombic and Lennard−Jones potentials, respectively, and the index k runs through all the water molecules present in the system. The last two terms add a repulsion between the solvent water oxygen atoms and hydronium oxygen and hydrogens. The $V^{\text{rep}}(R_{OO_k})$ term is given by

$$V^{\text{rep}}(R_{OO_k}) = B \exp[-b(R_{OO_k} - d^0_{OO})] \quad (5)$$

and $V^{\text{rep}}(R_{OH_k})$ is expressed as

$$V^{\text{rep}}(R_{OH_k}) = C \exp[-c(R_{OH_k} - d^0_{OH})] \quad (6)$$

Both repulsive potential terms are cut off using a cubic spline at a certain distance away from the hydronium oxygen. In the case of $V^{\text{rep}}(R_{OO_k})$, the cutoff is at 3.05 Å with the smoothing starting at 2.85 Å, while for $V^{\text{rep}}(R_{OH_k})$ the smoothing cutoff is at 3.00 Å starting at 2.50 Å. The exchange interaction charges on oxygen atoms along with several parameters in the EVB coupling elements were also adjusted. Those parameters of the MS-EVB2 hydronium model that differ from the original MS-EVB model[17] for the hydrated proton are listed in Table 1.

TABLE 1: Weak Acid MS-EVB Model Parameters for Matrix Elements Involving the Hydronium States Different from Ref 17

$\epsilon_O^{H_3O^+}$	0.1008 kcal mol^{-1}
$\sigma_O^{H_3O^+}$	3.14 Å
B	14.014 kcal mol^{-1}
b	2.20 Å^{-1}
d^0_{OO}	2.40 Å
C	7.387 kcal mol^{-1}
c	3.60 Å^{-1}
d^0_{OH}	0.98 Å
α	12.0 Å^{-1}
r^0_{OO}	1.88 Å
V^{ij}_{const}	−32.419 kcal mol^{-1}
q^{ez}_O	−0.116725 e
q^{ez}_H	−0.04669 e

C. Imidazolium VB State. The acid−water VB state (ImH^+-H_2O in this work) has also been slightly modified from the previous study.[19] For the sake of completeness, we describe the model in full detail here, although many aspects of the model are the same as those in the recent publication.[19]

The diagonal matrix element corresponding to the ImH^+ and its interaction with the hydration water molecules (state $|2\rangle$ in Figure 1) is described as

$$h^{ImH^+}_{ii} = \sum_k^{N_{H_2O}+1} V^{\text{intra},k}_{H_2O} + \sum_{k<k'}^{N_{H_2O}+1} V^{\text{inter},kk'}_{H_2O} + V^{\text{intra}}_{ImH^+} + \sum_k^{N_{H_2O}+1} V^{\text{inter},k}_{H_2O,ImH^+} + V^{\text{rep}}_{\text{const}} \quad (7)$$

Similar to the hydronium VB state, the inter- and intramolecular potential parameters involving the imidazolium molecule are the same as those for the protonated histidine residue[33] in the CHARMM 24 force field.[35] The atomic charges on imidazolium were, as in the imidazole case, taken from the Merz−Kollman electrostatic charge distribution calculated at the HF/6-31G* level.[36] A schematic picture of this VB state with associated point charges is depicted in the lower panel of Figure 1. The new set of charges on the imidazolium atomic centers, together with the CHARMM Lennard-Jones and intramolecular parameters, was found to improve the agreement of the geometry and H-bond energy of small ImH^+−water clusters, with respect to

TABLE 2: Weak Acid MS-EVB Model Parameters for the Imidazolium VB State Diagonal Matrix Elements

$V_{\text{const}}^{\text{rep}}$	-76.29 kcal mol^{-1}
V_{const}^{ij}	-44.17 kcal mol^{-1}
r_{sc}^{0}	1.08 Å
r_{NO}^{0}	2.60 Å
α_I	2.02 Å^{-2}
a_{NO}	3.30 Å
β_{I}	4.10 Å^{-2}
b_{NO}	2.00 Å
ϵ_{I}	13.00 Å^{-1}
c_{NO}	2.40 Å
γ_{I}	4.50 Å^{-2}

the reference ab initio values. The parameters for the solvent water molecules are the same as those in the hydronium VB states described above.

The constant term $V_{\text{const}}^{\text{rep}}$ is included to callibrate the energy difference between the hydronium and imidazolium in their global potential minima. The large stabilization of the hydronium states as compared to the imidazolium state is mainly caused by the short-range Coulombic interactions between the donor nitrogen of the imidazole and the acceptor hydrogens of the adjacent hydronium molecule.

The off-diagonal elements for the water$-$ImH$^+$ coupling are modeled as

$$h_{ij}^{\text{ImH}^+} = V_{\text{const}}^{ij} A(R_{\text{NO}},q) \tag{8}$$

where q is the proton-transfer coordinate

$$q = R_{\text{NH}} - \frac{R_{\text{NO}}}{2} r_{\text{sc}} \tag{9}$$

and r_{sc} is a scaling factor used to introduce the asymmetry of the PT potential into the coupling term, given by

$$r_{\text{sc}} = r_{\text{sc}}^{0} - \frac{R_{\text{NO}} - r_{\text{NO}}^{0}}{15} \tag{10}$$

The functional form of $A(R_{\text{NO}},q)$ in eq 8 is taken as the product of functions

$$A(R_{\text{NO}},q) = f(R_{\text{NO}})g(q) \tag{11}$$

where

$$f(R_{\text{NO}}) = [\exp(-\alpha_{\text{I}}(R_{\text{NO}} - a_{\text{NO}})^2) + \exp(-\beta_{\text{I}}(R_{\text{NO}} - b_{\text{NO}})^2)] \times [1 + \tanh(\epsilon_{\text{I}}(R_{\text{NO}} - c_{\text{NO}}))] \tag{12}$$

and

$$g(q) = \exp(-\gamma_{\text{I}} q^2) \tag{13}$$

All of the adjustable parameters entering into the protonated weak acid EVB state potential were systematically fit to reproduce select ab initio energetic and geometric features of the system under consideration and are listed in Table 2. Details on the fitting procedure are presented in the next section.

The interaction topology of the additional imidazolium VB state with the other VB states was constructed as follows: The algorithm searches for hydrogens within a certain radius from the donor nitrogen atom (2.25 Å in the current parametrization). Then it locates the closest oxygen atom to this hydrogen. If this oxygen belongs to a water molecule already included in the EVB description, the VB state with this hydrogen atom being the transferring proton is accepted as a new VB state. The remaining water topology for this new state is taken from the hydronium VB state which donated its proton to the imidazole. This procedure ensures that the imidazolium proton can only be transferred to water molecules included in the EVB complex. Note that more than one imidazolium VB states can thus be generated for a given configuration, as there can be more than one hydrogen atom belonging to an EVB complex water molecule located within the cutoff distance from the N donor atom. However, this case is rarely observed, mainly due to the geometrical restrictions imposed by the 3-dimensional hydrogen-bond network of the protonated hydration shell. As the hydronium VB states are generated up to a third solvation shell of the imidazole, a total of 5$-$7 hydronium and one imidazolium VB state are typically used during the course of the simulation.

TABLE 3: Hydrogen Bond Energies and $V_{\text{const}}^{\text{rep}}$ Term of Selected ImH$^+-$(H$_2$O)$_n$ Clusters (all in kcal/mol)

	MS-EVB	HF/6-31G*	MP2/6-31G*	$V_{\text{const}}^{\text{rep}}$
ImH$^+-$H$_2$O	-18.11	-16.95	-20.13	-74.13
ImH$^+-$(H$_2$O)$_2$	-30.45	-29.16	-35.08	-76.26
ImH$^+-$(H$_2$O)$_3$	-40.80	-39.37	-47.97	-80.54

3. MS-EVB Model Parametrization

A. Ab inito Calculations. The MS-EVB PES for the proton transfer from imidazolium to a hydrated water molecule was fitted in part to data from ab initio electronic structure calculations. The number of water molecules solvating the imidazole ranged from one to four in these studies. The reference data were recently reported in an ab initio study of PT in the carbonic anhydrase.[31] There, the ImH$^+-$water cluster geometries were optimized at the HF/4-31G level at several points along the ImH$^+-$OH$_2$ PT coordinate, and these geometries were used to calculate MP2/4-31 g energies.

Although the earlier calculations gave a good qualitative picture of the PT energetics of these systems, it is desirable to obtain an even more reliable PT PES to which to fit the MS-EVB model. Therefore, we recalculated the PT PES for the ImH$^+-$(H$_2$O)$_n$ (n = 1$-$3) water clusters at a higher level of theory. Geometries of the global minima of these clusters and of selected points along the PT coordinate were optimized at the MP2/6-31G* level with frozen core electrons. This set of data served as the new reference ab initio PT PES. During the optimization, all the atomic coordinates were relaxed except for the planarity restriction on the imidazole ring and the specified R(NO) and R(NH) distances, with N being the proton donor, O the proton acceptor, and H the transferring proton. Similar to the work by Nagy et. al.,[25] we found that electron correlation has a relatively large influence of the optimized geometry of the PT system. Also non-negligible was the potential energy decrease of the product proton transferred species (imidazole$-$hydronium) relative to the imidazolium$-$water minimum upon the MP2 geometry optimization. Hydrogen bond energies and selected geometric features of the studied ImH$^+-$(H$_2$O)$_n$ clusters are reported in Tables 3 and 4. The PT potential energy curves as a function of the NH and NO distance are displayed in Figure 2. Both the two tables and Figure 2 are discussed in more detail below. All the ab initio calculations were performed using the Gaussian98 program package.[36]

B. MS-EVB Potential Fitting Procedure. The MS-EVB PT potential for the ImH$^+-$(H$_2$O)$_n$ (n=1$-$3) was obtained by a

TABLE 4: Selected Geometry Parameters (bonds in Å, angles in deg) of Selected $ImH^+-(H_2O)_n$ Clusters

		EVB	HF/6-31G*	MP2/6-31G*
r(NH)	ImH^+-H_2O	1.056	1.015	1.043
	$ImH^+-(H_2O)_2$	1.063	1.022	1.059
	$ImH^+-(H_2O)_3$	1.069	1.030	1.084
r(NO)	ImH^+-H_2O	2.704	2.819	2.748
	$ImH^+-(H_2O)_2$	2.678	2.748	2.667
	$ImH^+-(H_2O)_3$	2.657	2.689	2.600
θ(NHO)	ImH^+-H_2O	177.5	178.0	176.4
	$ImH^+-(H_2O)_2$	176.7	171.5	171.1
	$ImH^+-(H_2O)_3$	175.6	169.3	170.9

simulated annealing protocol from the gas-phase cluster which was cooled to 0 K for predefined fixed *R*(NH) and *R*(NO) distances. The strong dependence of the PT barrier height on the distance between the proton donor and acceptor is well-known,[37−39] a feature that should be reproduced by any EVB parametrization. Four different fixed NO distances of 2.45, 2.60, 2.75, and 2.90 Å were used, and the proton in each case was moved from the ImH^+ molecule to the nearest water by steps of 0.1 Å. The fitting procedure involved the determination of an appropriate functional form for the EVB state coupling term and the VB state energy difference $V_{\text{const}}^{\text{rep}}$. Particular attention was paid to an accurate reproduction of the PES in the transition state region. As the imidazolium−water NO distance decreases from 2.75 Å in ImH^+-H_2O to 2.60 Å in $ImH^+-(H_2O)_3$ (see Table 4), good fits at *R*(NO) = 2.60 and 2.75 Å are more important. The fits at small *R*(NO) = 2.45 Å and large *R*(NO) = 2.90 Å were conducted mainly in order to obtain qualitatively correct potential behavior at the H-bond geometry limits. Still, the ab initio potential even in these cases is reproduced to within a few kilocalories per mole.

The ab initio potential surface for clusters containing 1−3 water molecules relative to the global minimum of a distinct cluster is displayed in Figure 2. For the sake of clarity, we did not include the potential curves with *R*(NO) = 2.45 and 2.90 Å. Also, note that the PES curves at *R*(NO) = 2.60 Å are artificially shifted upward by 10 kcal/mol to make the figures easier to interpret. All three figures display no barrier for the reverse PT at *R*(NO) = 2.60 Å, although for clusters containing three water molecules, there is an obvious plateau. At *R*(NO) = 2.75 Å, the $n = 3$ cluster displays a clear minimum for the PT state. Adding waters to the imidazolium lowers the relative energy of the PT species at *R*(NO) = 2.60 Å from ca. 26.7 kcal/mol for $n = 1$ to 15.3 kcal/mol for $n = 2$ to 6.6 kcal/mol for $n = 3$. A similar trend is exhibited at other *R*(NO) distances as well. The MS-EVB model reproduces the ab inito potential reasonably well, taking into consideration that a fit in a highly dimensional parameter space for a complex PES had to be performed.

To check for correct MS-EVB model behavior at the $ImH^+-(H_2O)_n$ limit, we MD-quenched small gas-phase $n = 1-3$ clusters without any geometry restrictions using the parameter set obtained by the fitting procedure described above. The H-bond energies for the MS-EVB method are compared with the ab initio results in Table 3. The MS-EVB reproduces well the ab initio formation energies, somewhere between the HF and MP2 results. The ImH^+-OH_2 H-bond geometry parameters of these clusters reported in Table 4 are also found to lie between the HF and MP2 results. Notice the decrease in the *R*(NO) distance and increase in *R*(NH) distance with increasing number of water molecules in the cluster, consistent with a lowering of the PT barrier and enthalpy of the PT reaction, as evident from Figure 2.

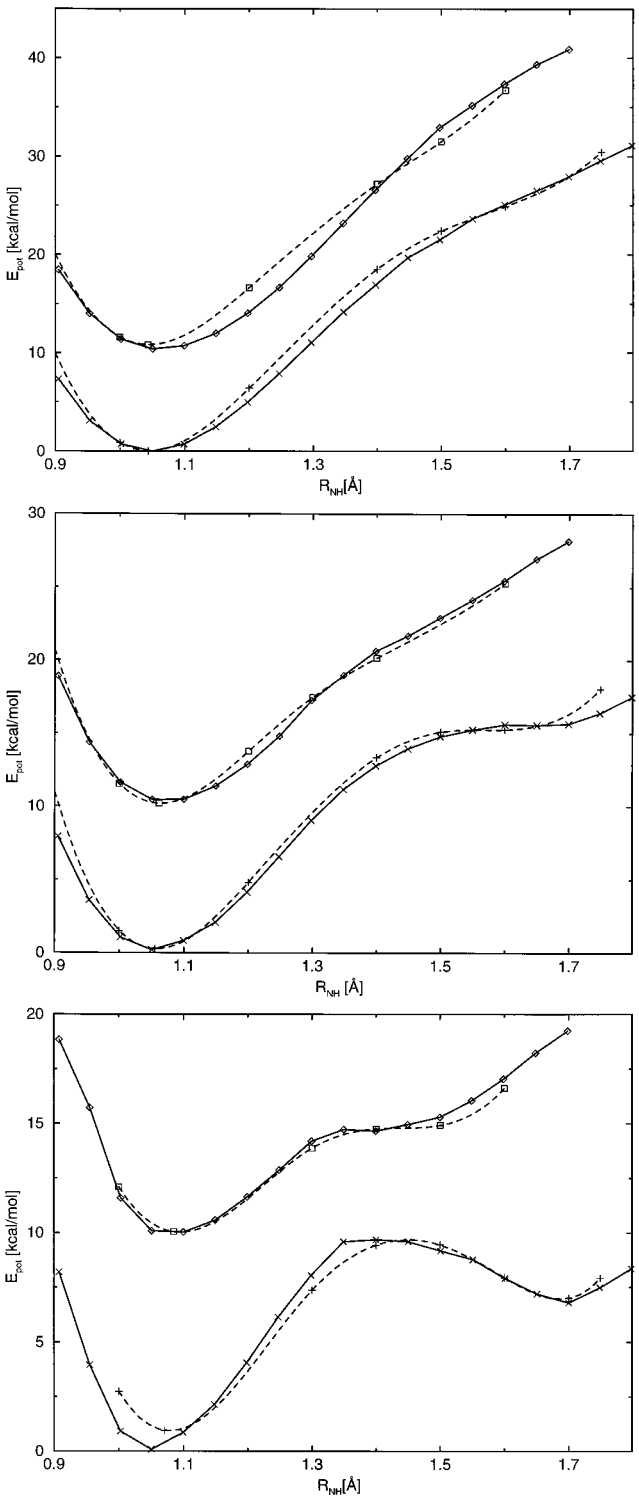

Figure 2. Potential energy surface for PT from imidazolium to hydronium calculated by the MS-EVB (full lines) and ab initio (dashed lines) at *R*(NO) = 2.75 and 2.60 Å (artificially shifted up by 10 kcal/mol) for (a) ImH^+-H_2O, (b) $ImH^+-(H_2O)_2$, and (c) $ImH^+-(H_2O)_3$. The ab initio energies are relative to the energy of the global minimum of the particular ImH^+−water cluster.

C. Free Energy of Reaction. It is a challenge to correctly reproduce both the PT barrier and the reaction free energy (ΔF) in solution. A thorough parametrization of small weak acid−water clusters in the gas phase will identify the trend into the solution and help to obtain correct deprotonation reaction energetics for the weak acid when it is immersed in an explicit water solvent. As mentioned above, since the reaction PES is

asymmetric, a correct determination of the energy difference, $V_{\text{const}}^{\text{rep}}$, between the VB states entering in this model (imidazolium and hydronium) is of crucial importance. A complication in the determination of the term $V_{\text{const}}^{\text{rep}}$ in the model stems from the observation that with an increasing number of water molecules around the water molecule H-bonded to the weak acid, the $V_{\text{const}}^{\text{rep}}$ term has to be increased in order to obtain an accurate reproduction of the ab initio hydration PES. The values of $V_{\text{const}}^{\text{rep}}$ we used for the $n = 1-3$ gas-phase cluster PES fitting and comparison to the ab initio results are reported in the last column of Table 3.

The necessity to increase the $V_{\text{const}}^{\text{rep}}$ term with increasing number of waters in the cluster arises from an increased stabilization of the positively charged hydronium molecule in the hydronium VB state, due to the large hydration energy of the hydronium ion. Conversely, in the imidazolium VB state, the positively charged imidazolium molecule is still mainly solvated only by one of the first solvation shell water molecules which is hydrogen bonded to the donor H atom. One can therefore expect a similar energetic stabilization of the imidazolium VB state as it gets solvated further. Unfortunately, we were unable to extract the fully hydrated form of the imidazolium VB state due to the fact that during the simulated annealing process the adiabatically added water molecules tend to migrate toward the hydronium molecule rather than solvate other imidazolium residue atoms, as they would in the full liquid-state environment. Thus, to determine the final value of $V_{\text{const}}^{\text{rep}}$, we calculated several short umbrella sampling simulations with the simulation box containing the imidazolium molecule and solvent water (cf. details in the next section) and varied the value of $V_{\text{const}}^{\text{rep}}$ to obtain the correct value of ΔF.

The experimental free energy of reaction, as discussed in our previous work,[19] can be calculated from the pK_a of the reacting species and is found to be equal to 11.8 kcal/mol. We have also compared this experimental value to that obtained from an ab initio calculation. Harmonic zero-point energy and the thermal energy corrected free energy from the Gaussian98[36] frequency output was used to obtain a free energy estimate of the reacting species in the gas phase. The free energy of the ImH^+ deprotonation reaction in the gas phase was then calculated as a difference in free energies of the products and reactants, yielding a value of 57.9 kcal/mol. The sum of free energies of solvation of the dissociated species involved in the reaction, calculated using the Polarizable Continuum Model,[40] yields −46.7 kcal/mol for the reaction. The free energy of the reaction in the solution was then estimated to be the sum of the free energy of the reaction in a gas phase and the solvation free energy difference between the reactants and products. This way, the free energy of the imidazolium deprotonation in the solution is estimated to be 11.3 kcal/mol, in close agreement with the experimental value. Considering the free energies of reaction obtained above, together with the short umbrella sampling simulations results, a value for the $V_{\text{const}}^{\text{rep}}$ term of −76.29 kcal/mol was found to give the best fit to the experimental results. We note that this value is very close to that obtained from the an initio fitting procedure for the case of $ImH^+-(H_2O)_2$ listed in Table 3.

4. Methods of Simulation

All the calculations described below were performed in a classical MD simulation framework. The ImH^+ molecule was immersed in a cubic simulation box ($L = 17.83$ Å) containing 186 water molecules, which corresponds to molar acid concentration of 0.29 M. (We note that no counterion was contained in this simulation, which should be a reasonable approximation in this relatively low concentration limit.) Periodic boundary conditions were employed and the long-range Coulombic forces were treated with Ewald summation.[41] A real-space screening factor of $\kappa = 6.3/L$ was used, and the k-space was expanded in a total of 1664 k-vectors. The Lennard-Jones intermolecular potential was smoothed to zero at the $L/2$ distance using a spline function. The MD time integration step within the Verlet integrator was 0.5 fs in all simulations reported.

To obtain the free energy along selected degrees of freedom for the ImH^+ deprotonation, we used the umbrella sampling technique.[42,43] In our previous work, the geometric proton-transfer coordinate q as defined in eq 9 was used as the reaction coordinate for the umbrella potential with the scaling factor r_{sc} set to unity. However, we found that at $q > 0.2$ Å, corresponding to the Im-hydronium state $|1\rangle$ in Figure 1, the excess proton is often seen to oscillate between the hydronium and its first solvation shell waters. This increases both statistical and systematic error in the free energy because a large portion of phase space has to be explored while the value of PT coordinate remains relatively fixed due to the umbrella potential. Also, the shuttling of the proton to other waters via the Grötthus mechanism can be improperly constrained.

Therefore, it is desirable to use a different PT coordinate that more generally describes the movement of the charge associated with the excess proton away from the imidazole molecule. The option chosen in this work was to define the PT coordinate (and with it the umbrella sampling reaction coordinate) as the difference between the center of excess charge (CEC) of the full MS-EVB complex and the nitrogen proton donor atom of the imidazole molecule. The CEC reaction coordinate is thus expressed as

$$q_{\text{CEC}} = |\mathbf{x}_{\text{CEC}} - \mathbf{x}_{\text{N}}| \tag{14}$$

where $\mathbf{x}_{\text{N}}$ is the imidazole nitrogen atom donor position and $\mathbf{x}_{\text{CEC}}$ is the center of excess protonic charge defined as

$$\mathbf{x}_{\text{CEC}} = \sum_{i=1}^{N_{\text{EVB}}} c_i^2(\mathbf{x})\mathbf{x}_i^{\text{COC}} \tag{15}$$

In this relation, $c_i^2(\mathbf{x})$ is the amplitude of EVB state i, and $\mathbf{x}_i^{\text{COC}}$ is the center of charge of the hydronium in a given hydronium EVB state or a center of charge of the donor nitrogen and transferring proton atoms in the case of the imidazolium EVB state. There is a total of N_{EVB} possible MS-EVB states. The value of the CEC PT coordinate varies from around 0.65 Å in the case when the excess proton is localized on the imidazolium molecule to 2.6−3.0 Å when it is on the hydronium adjacent to the imidazole. Values larger than 3.0 Å correspond to the proton diffusing (or "hopping") into the aqueous phase.

The umbrella potential was chosen to be of harmonic form, given by

$$V_{\text{umbrella}}^{i}(q_{\text{CEC}}) = \frac{k}{2}(q_{\text{CEC}} - q_0)^2 \tag{16}$$

Since the gradient of the proton transfer potential varies considerably with the q_{CEC} coordinate, the force constant k was adjusted so that a satisfactory number of samples were accepted in each window. For each window, individual trajectories were equilibrated for 25 ps, and the data was collected in the NVT ensemble[44] for a period of 150 ps. A total of 60 umbrella windows were used, spanning the range $q_0 = 0.65$ Å−3.60 Å,

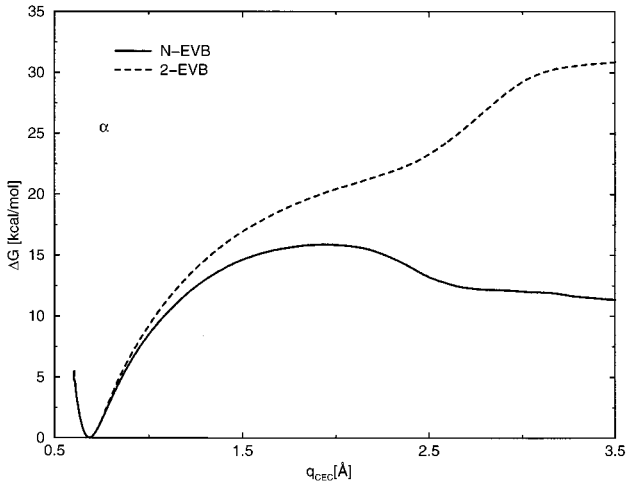

Figure 3. Imidazolium deprotonation free energy plot as a function of the center of excess charge coordinate q_{CEC} for the N-EVB (full line) and 2-EVB (dashed line) models.

with a window size of 0.35 Å. The constant temperature weighted histogram analysis technique (WHAM),[45] as modified by Roux,[46] was used to match the individual umbrella windows and to obtain a continuous free energy (FE) curve. A second umbrella sampling simulation was computed using just a two-state EVB (2-EVB) model, comprising only of states $|1\rangle$ and $|2\rangle$ as shown in Figure 1, solvated by TIP3P water. No additional hydronium states were allowed on nearby water molecules. This allows one to assess the effect of hydronium solvation, polarization, and shuttling by the surrounding solvent on the proton-transfer free energy profile.

Another point of interest is the influence of the solvated protonated imidazole (ImH^+) and its neutral form (Im) on the solvent, in particular the equilibrium and dynamic properties of the water solution in the presence of the solute and the possibility of proton shuttling from the weak acid ion pair into the solution. Both simulations were computed using the N-state EVB model. In this case, the system was thermalized at 300 K for 50 ps, followed by 50 ps equilibration and 200 ps constant energy data collection. One simulation focused on the imidazolium, while another on the imidazole. Five trajectories with independent initial conditions were used in each case. Since the PT barrier is relatively high in both directions, no reactive event was observed involving the imidazole molecule. The energy conservation in both imidazolium−water and imidazole−hydronium−water systems was reasonably good with energy drift of about 1.5% per 100 ps.

5. Results and Discussion

A. Imidazolium Free Energy of Deprotonation. The free energy curves for the PT reaction along the center of excess charge reaction coordinate for both the N-EVB and 2-EVB models are displayed in Figure 3. The N-EVB curve shows a solvent-induced stabilization of the product species with a reaction free energy $\Delta F = 12.00$ kcal/mol. The proton-transfer barrier in the forward direction is 15.95 kcal/mol. Note the flattened area on the N-EVB free energy curve in the product region at $q_{CEC} \geq 2.7$ Å. At this distance, the excess proton is fully transferred and is bound to the Im first solvation shell water molecule. Further movement along the reaction coordinate results in reorganization of the solvent around the imidazole molecule and shuttling of the excess proton into the solution. In contrast to the N-EVB model, the 2-EVB curve shows no minimum in the product hydronium region, as there are no other

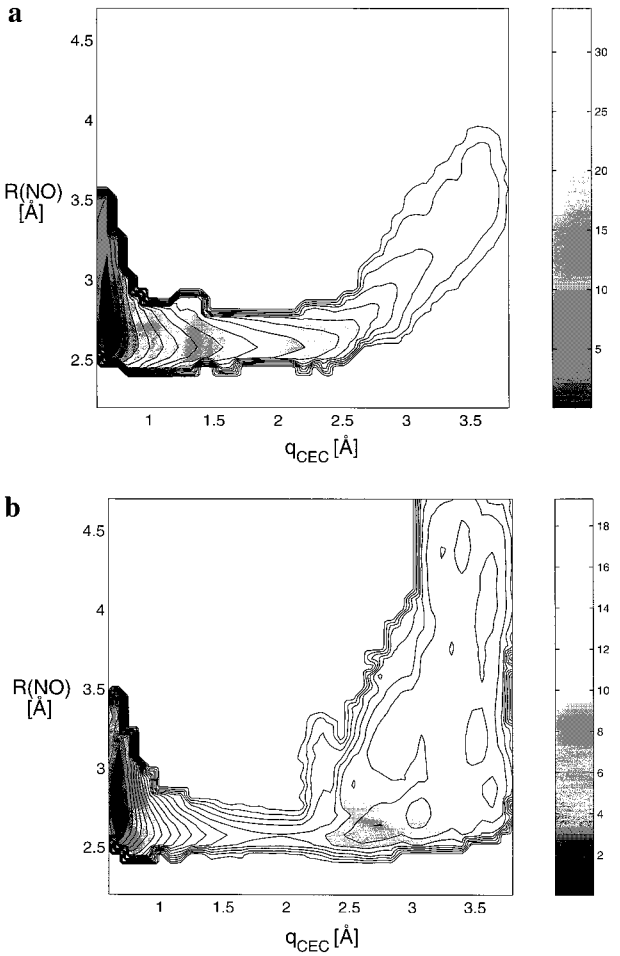

Figure 4. 3D plot of the imidazolium deprotonation free energy surface as a function of the center of excess charge coordinate q_{CEC} and the distance between the nitrogen donor atom and dominant hydronium EVB state oxygen atom, R(NO), using (a) the 2-EVB model and (b) the N-EVB model.

water−hydronium VB states that would stabilize the product through proton shuttling. Thus, the 2-EVB free energy curve continues to rise to about $q_{CEC} = 3.0$ Å, and only past this value does it somewhat flatten. This flattening can again be related to the excess charge diffusing into the aqueous solution, though by a classical diffusion mechanism. A comparison of these two curves shows the very significant influence of the proton shuttling on the weak acid dissociation process.

A complementary picture of the PT process can be obtained from a composite 3D free energy plot relating two variables, the center of excess charge and the distance R(NO) between the nitrogen donor atom and the oxygen acceptor. The acceptor is here defined as the oxygen atom belonging to the water with the largest hydronium EVB state amplitude. The free energy was calculated similarly to that in our previous work,[19] using the probability density $p[q_{CEC},R(NO)]$ and adjusting the free energy for each umbrella window by the window shift coefficient obtained from the WHAM window adjustment algorithm.

The composite free energy plot is displayed in Figure 4 (upper panel corresponds to the 2-EVB model, lower panel to N-EVB). The left part of the plot up to about $q_{CEC} = 1.5$ Å is similar in the two models, suggesting that the imidazolium solvation is sufficiently desribed here by the inclusion of just one hydronium EVB state. On the other hand, the product regions of the two plots differ dramatically. While no product stabilization can be seen in the 2-EVB case, the N-EVB plot reveals a large basin

at $q_{CEC} > 2.5$ Å, corresponding to hydrated proton stabilized by the solvent. Note the several shallow minima in this region as the R(NO) increases. These correspond to more localized positions of the hydronium oxygens as the proton shuttles away from the nitrogen atom donor into the solution. There appears to be a very small barrier for the proton to shuttle further into solution, in accord with the previous simulation results of the protonated water solution.[16−18]

Further insight into the microscopic details of the system during and after the initial proton-transfer step can be obtained by examining the changes in the amplitudes of various VB states, c_i^2, along the reaction coordinate. A plot of the free energy surface as a function of the composite coordinate c_i^2 and q_{CEC} for the N-EVB system is shown in Figure 5. The free energy was calculated the same way as mentioned above, using the probability density $p(q_{CEC},c_i^2)$. The c_i^2 in panel a of Figure 5 represents the amplitude of the imidazolium VB state. It is nearly unity on the left side of the reaction coordinate, when this state dominates, but it approaches zero at $q_{CEC} > 2.6$ Å. In the panels b and c of Figure 5, the c_i^2 coordinates represent the amplitudes of the first and second most dominant hydronium VB states. In the reactant region, the dominant hydronium VB state amplitude is close to zero, and it rises continuously as the proton moves away from the imidazole. From the reactant state to the start of transition region at ca. $q_{CEC} = 1.5$ Å, the sum of this hydronium and the imidazolium states VB amplitudes is close to unity, since the other VB states couple only weakly with the reacting system. The most dominant hydronium state represents the hydronium molecule that is being formed by the ImH^+ deprotonation. The probablility distribution of the EVB amplitude of this state in the product region displays a maximum of about 0.75 at $q_{CEC} = 2.6$ Å. Such a large VB amplitude signals a preference for an Eigen-like species solvated evenly by the Im and two surrounding waters. As the CEC moves further away from the Im, however, the average amplitude of this EVB state slowly decreases. This reduction is caused by the delocalization of the excess proton charge to the other VB states that solvate the first solvation shell hydronium, which become increasingly populated as the center of excess charge moves away from the N atom donor. Consequently, the amplitude of the second most dominant hydronium VB state increases from zero in the transition state region to ca. 0.20 in the product area. The decrease of the dominant hydronium VB state amplitude in the product region signals a rising Zundel-like contribution as the CEC moves away from the imidazole to the limit that is seen in the bulk water simulation results.[17]

Since the proton transfer away from the initial hydronium proton acceptor is enabled in the MS-EVB model, the proton is free to transfer further into the solution. The index of the dominant hydronium can thus change over the trajectory run. On the other hand, this transfer is limited by the presence of the umbrella potential that fixes the distance between the CEC and the N donor atom, which enables us to observe continuous movement of the proton from the imidazolium molecule into the water solution.

B. Solvation Structure of the Imidazolium/Imidazole. While a more detailed examination of the weak acid deprotonation mechanism will be the subject of a subsequent study, it is instructive to inspect the water solvation structure around the imidazole molecule in both the protonated and neutral states. As the imidazole molecule has only one plane of symmetry, radial distribution functions, which rely on the spherical or cylindrical symmetry around the atoms of interest (in our case the N donor), do not provide a completely adequate description.

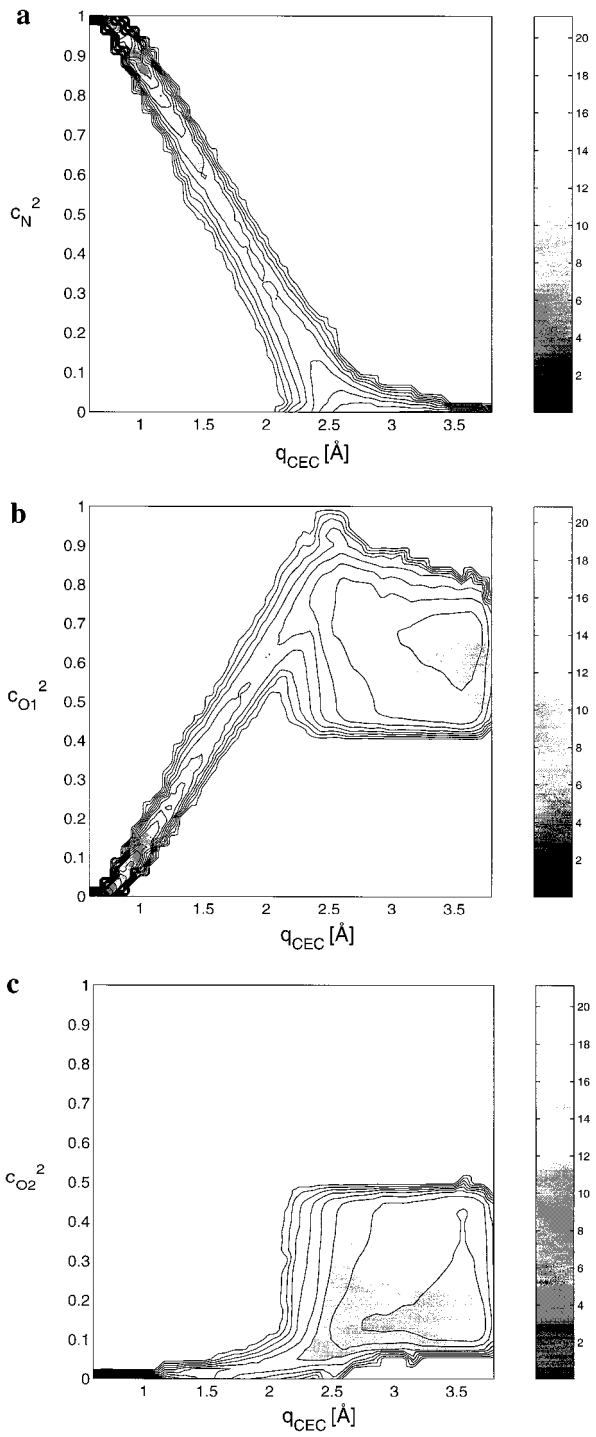

Figure 5. 3D plot of the imidazolium deprotonation free energy surface as a function of the center of excess charge coordinate q_{CEC} and VB amplitude c_i^2 of (a) the imidazolium, (b) the most dominant hydronium, and the second most dominant hydronium (c) VB state using the N-EVB model.

A projection of the nuclear densities on a 3-D grid provides an alternative for inspecting the microscopic situation from the simulation. For each of the umbrella windows, we sampled the nuclear density distribution around the imidazole molecule, with the coordinates in the simulation box transformed at each time step so that the imidazole molecule lies in the *xy* plane and the N donor is at the center of the box. The plots in Figure 6 show areas with the atomic density four times the average density in the simulation box or greater. When the proton is bound to the imidazole (such as at $q_{CEC} = 0.7$ Å in Figure 6a), the atom

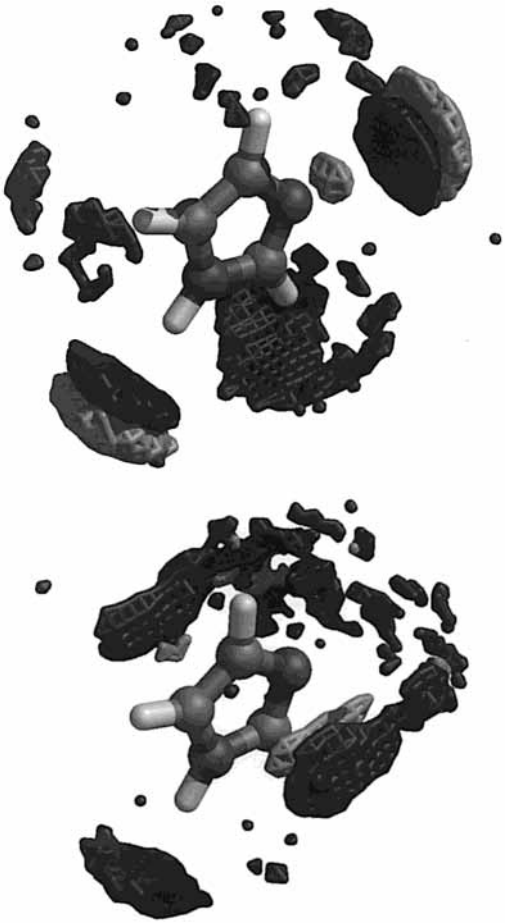

Figure 6. Atom density plot for the normalized hydrogen and oxygen atomic distribution around the imidazole molecule: (a) $q_{CEC} = 0.70$ Å and (b) $q_{CEC} = 3.00$ Å. Oxygen density in dark gray and hydrogen density in light gray.

density plot indicates a clear "one water molecule" solvation pattern on both imidazole N atoms (recall that only one of these nitrogen atoms is allowed to be a proton donor in our MS-EVB model). The positions of these density maxima are localized in a conical distribution around the NH axes. The spherical hydrogen density pattern close to the N donor in Figure 6a represents the proton bound to this nitrogen. A less populated oxygen density area can be seen in the proximity of the other hydrogen atoms bound to the imidazolium ring. There is no distinct area with high water density located off the imidazolium molecular plane.

In the neutral imidazole, the water (oxygen) density distribution around the protonated N atom (which does not take part in the PT) remains almost unchanged. On the other hand, the probability density of the water molecules (and hydronium) around the N donor ($q_{CEC} = 2.6$ Å in Figure 6b) is more delocalized, with a distribution reaching further away from the imidazole molecule plane. This area of high water probability density represents the VB complex of the hydronium ion and its hydrating water molecules. With an increasing CEC reaction coordinate, a distinct rise in the water population density above and below the imidazole plane can be observed. There is one water molecule hydrating each side, which is not included in the VB complex. One hydrogen atom of each of these waters is oriented toward the negative point charges other than nitrogen atoms in the Im ring. Since the sum of ring point charges in the protonated Im is much less negative than that in the neutral Im, this pattern is not observed in Figure 6a.

C. Dynamics of the PT in the Presence of Imidazolium/Imidazole. To compare the dynamic properties of the solution containing the imidazolium or imidazole molecule with the hydrated proton solution without the solute, we performed two microcanonical ensemble simulations. One focused on the solvated ImH^+-H_2O system and the other on $ImH^+-H_3O^+$. Due to a large PT barrier, the simulation of the imidazolium solvated in water did not produce any proton transfer to the solvent waters. The proton stays bound to the nitrogen atom donor throughout the course of simulation, with the imidazolium VB state amplitude around 0.99. The water diffusion constant increases slightly with the presence of the imidazolium molecule to 0.34 ± 0.04 Å^2 ps^{-1}. Disruption of the water hydrogen bonded structure around the ImH^+ coupled with the excess charge on the imidazolium is the most likely cause for this increase. On the other hand, since the excess charge is located on the imidazolium, the CEC diffusion reflects that of the larger imidazolium molecule and is only 0.17 ± 0.06 Å^2 ps^{-1}.

Also in the simulation of the neutral imidazole in the protonated water solution, we did not observe any reverse proton transfer toward the nitrogen atom donor. The water diffusion constant is within the error bars of the imidazolium-water solution at 0.32 ± 0.02 Å^2 ps^{-1}. The center of excess charge diffusion constant, having a value 0.35 ± 0.12 Å^2 ps^{-1}, matches a result obtained in the pure protonated water simulation using the full-charge MS-EVB model. The rather low concentration of the weak acid conjugate base in the solution has also very small effects on transfer rates of the excess proton in the solvent at the limit of statistical resolution. These observations, showing a very small effect of the solute in small concentrations on the PT of the excess proton in the water solution, are in accord with those noted in our previous work[19] that examined a Cl^- anion solution in the protonated water.

6. Conclusions

A multistate empirical valence bond model for the dissociation of a weak acid molecule in water has been described in this paper. To express more generally the charge interactions between the protonated water solution and the weak acid conjugate base, our original MS-EVB model for the hydrated proton has been modified. The weak acid MS-EVB model was applied to study the imidazolium cation deprotonation reaction. The model was first parametrized to describe accurately the potential energy surface of the imidazolium deprotonation in small ImH^+-H_2O clusters. Molecular dynamics simulations together with umbrella sampling were then performed in order to obtain the free energy surface relevant to the PT process in the bulk phase. The free energy of reaction is found to be 12.00 kcal/mol, with a forward PT barrier height of 15.95 kcal/mol. This result was compared with a reduced EVB model involving only two VB states, those of the ImH^+ proton donor and first solvation shell water molecule acceptor. This model shows no minimum in the hydronium product region, indicating the importance of the proton charge delocalization and shuttling into the hydration shells of the aqueous solution—a feature that can be only captured by a multistate description. While the imidazolium shows a relatively localized solvation pattern with a water density mainly around the two N−H groups that can act as proton donors, the water structure is more delocalized around the neutral imidazole. Wider water density patterns are observed around the nitrogen atoms and, additionally, above and below the aromatic ring. Finally, both equilibrium and dynamic parameters of the PT in the protonated water solution are found to be almost unaffected by the presence of the imidazole molecule at these concentrations.

Acknowledgment. This work was supported by the National Institutes of Health (Contract No. GM-53148) and the National Science Foundation (Contract No. CHE-9712884). M.C. would like to thank Mark Brewer for stimulating discussions.

References and Notes

(1) Bell, R. P. *The Proton in Chemistry*, 2nd ed.; Cornell University Press: Ithaca, NY, 1973.
(2) Caldin, E. F., Gold, V., Eds. In *Proton-Transfer Reactions*; Chapman and Hall: London, 1975.
(3) Bountis, T., Ed. In *Proton Transfer in Hydrogen-Bonded Systems*; Plenum: New York, 1993.
(4) Muller, A., Ratajczak, H., Junge, W., Diemann, E., Eds. In *Electron and Proton Transfer in Chemistry and Biology*; Elsevier: New York, 1992.
(5) Allen, M. P.; Tildesley, D. J. *Computer Simulation of Liquids*; Clarendon Press: Oxford, 1987.
(6) Warshel, A. *Computer Modeling of Chemical Reactions in Enzymes and Solutions*; J. Wiley and Sons: New York, 1991.
(7) Ceperley, D. M. In *Simulations in Condensed-Matter Physics and Chemistry*; Binder, K., Ciccotti, G., Eds.; Editrice Compositori: Rome, 1996.
(8) Cournoyer, M. E.; Jorgensen, W. L. *Mol. Phys.* **1984**, *51*, 119.
(9) Jedlovszky, P.; Vallauri, R. *Mol. Phys.* **1998**, *93*, 15.
(10) Car, R.; Parrinello, M. *Phys. Rev. Lett.* **1985**, *55*, 2471.
(11) Laasonen, K.; Klein, M. L. *Mol. Phys.* **1996**, *88*, 135- -142.
(12) Coulson, C. A.; Danielsson, U. *Ark. Fysik* **1954**, *8*, 239.
(13) Mulliken, R. S. *J. Chim. Phys. (Paris)* **1964**, *61*, 20.
(14) Warshel, A.; Weiss, R. M. *J. Am. Chem. Soc.* **1980**, *102*, 6218.
(15) Åqvist, J.; Warshel, A. *Chem. Rev.* **1993**, *93*, 2523.
(16) Schmitt, U. W.; Voth, G. A. *J. Phys. Chem. B* **1998**, *102*, 5547.
(17) Schmitt, U. W.; Voth, G. A. *J. Chem. Phys.* **1999**, *111*, 9361.
(18) Schmitt, U. W.; Voth, G. A. *Isr. J. Chem.* **1999**, *39*, 483.
(19) Čuma, M.; Schmitt, U. W.; Voth, G. A. *Chem. Phys.* **2000**, *258*, 187.
(20) Vuilleumier, R.; Borgis, D. *J. Mol. Struct.* **1997**, *436*, 555.
(21) Vuilleumier, R.; Borgis, D. *Chem. Phys. Lett.* **1998**, *284*, 71.
(22) Vuilleumier, R.; Borgis, D. *J. Phys. Chem. B* **1998**, *102*, 4261.
(23) Vuilleumier, R.; Borgis, D. *J. Chem. Phys.* **1999**, *111*, 4251.
(24) Rashin, A. A.; Rabinowitz, J. R.; Banfelder, J. R. *J. Am. Chem. Soc.* **1990**, *112*, 4133.
(25) Nagy, P. I.; Durant, G. J.; Smith, D. A. *J. Am. Chem. Soc.* **1993**, *115*, 2912.
(26) Topol, I. A.; Tawa, G. J.; Burt, S. K.; Rashin, A. A. *J. Phys. Chem. A* **1997**, *101*, 10075.
(27) Ho, L. L.; A. D. MacKerell, J.; Bash, P. A. *J. Phys. Chem.* **1996**, *100*, 4466.
(28) Bash, P. A.; Ho, L. L.; A. D. MacKerell, J.; Levine, D.; Hallstrom, P. *Proc. Natl. Acad. Sci. U.S.A.* **1996**, *93*, 3698.
(29) Hummer, G.; Pratt, L. R.; Garcia, A. E. *J. Phys. Chem. A* **1998**, *102*, 7885.
(30) Christianson, D. W.; Fierke, C. A. *Acc. Chem. Res.* **1996**, *29*, 331.
(31) Lu, D.; Voth, G. A. *J. Am. Chem. Soc.* **1998**, *120*, 4006.
(32) Lu, D.; Voth, G. A. *Proteins* **1998**, *33*, 119.
(33) MacKerell, A. D. J.; Bashford, D.; Bellott, M.; Dunbrack, R. L. J.; Evanseck, J. D.; Field, M. J.; Fischer, S.; Gao, J.; Guo, H.; Ha, S.; Joseph-McCarthy, D.; Kuchnir, L.; Kuczera, K.; Lau, F. T. K.; Mattos, C.; Michnick, S.; Ngo, T.; Nguyen, D. T.; Prodhom, B.; Reiher, W. E., I.; Roux, B.; Schlenkrich, M.; Smith, J. C.; Stote, R.; Straub, J.; Watanabe, M.; Workiewicz-Kuczera, J.; Yinb, D.; Karplus, M. *J. Phys. Chem. B* **1998**, *103*, 3586.
(34) Besler, B. H.; Merz, K. M.; Kollman, P. A. *J. Comput. Chem.* **1990**, *11*, 431.
(35) Brooks, B. R.; Bruccoleri, R. E.; Olafson, B. D.; States, D. J.; Swaminathan, S.; Karplus, M. *J. Comput. Chem.* **1983**, *4*, 187.
(36) Frisch, M. J.; Trucks, G. W.; Schlegel, H. B.; Scuseria, G. E.; Robb, M. A.; Cheeseman, J. R.; Zakrzewski, V. G.; Montgomery, J. A.; Stratmann, R. E.; Burant, J. C.; Dapprich, S.; Millam, J. M.; Daniels, A. D.; Kudin, K. N.; Strain, M. C.; Farkas, O.; Tomasi, J.; Barone, V.; Cossi, M.; Cammi, R.; Mennucci, B.; Pomelli, C.; Adamo, C.; Clifford, S.; Ochterski, J.; Petersson, G. A.; Ayala, P. Y.; Cui, Q.; Morokuma, K.; Malick, D. K.; Rabuck, A. D.; Raghavachari, K.; Foresman, J. B.; Cioslowski, J.; Ortiz, J. V.; Stefanov, B. B.; Liu, G.; Liashenko, A.; Piskorz, P.; Komaromi, I.; Gomperts, R.; Martin, R. L.; Fox, D. J.; Keith, T.; Al-Laham, M. A.; Peng, C. Y.; Nanayakkara, A.; Gonzalez, C.; Challacombe, M.; Gill, P. M. W.; Johnson, B. G.; Chen, W.; Wong, M. W.; Andres, J. L.; Head-Gordon, M.; Replogle, E. S.; Pople, J. A. *Gaussian 98*; Gaussian, Inc.: Pittsburgh, PA, 1998.
(37) Pavese, M.; Chawla, S.; Lu, D.; Lobaugh, J.; Voth, G. A. *J. Chem. Phys.* **1997**, *107*, 7428.
(38) Sadhukhan, S.; Munoz, D.; Adamo, C.; Scuseria, G. *Chem. Phys. Lett.* **1999**, *306*, 83.
(39) Scheiner, S. *Acc. Chem. Res.* **1985**, *18*, 174.
(40) Miertuš, S.; Tomasi, J. *Chem. Phys.* **1982**, *65*, 239.
(41) Hummer, G.; Pratt, L. R.; Garcia, A. E. *J. Phys. Chem.* **1996**, *100*, 1206.
(42) Patey, G. N.; Valeau, J. P. *J. Chem. Phys.* **1975**, *63*, 2334.
(43) Pangali, C.; Rao, M.; Berne, B. *J. Chem. Phys.* **1979**, *71*, 2975.
(44) Kast, S. M.; Nicklas, K.; Bär, H.-J.; Brickmann, J. *J. Chem. Phys.* **1994**, *100*, 566.
(45) Kumar, S.; Bouzida, D.; Swendsen, R. H.; Kollman, P. A.; Rosenberg, J. M. *J. Comput. Chem.* **1992**, *13*(8), 1011.
(46) Roux, B. *Comput. Phys. Comm.* **1995**, *91*, 275.